Supplementary Material to Numerical simulations of mixed-mode (I and II) notch tip fields in basal-textured magnesium alloys

S1. Actual Texture for the rolled AZ31 Mg alloy

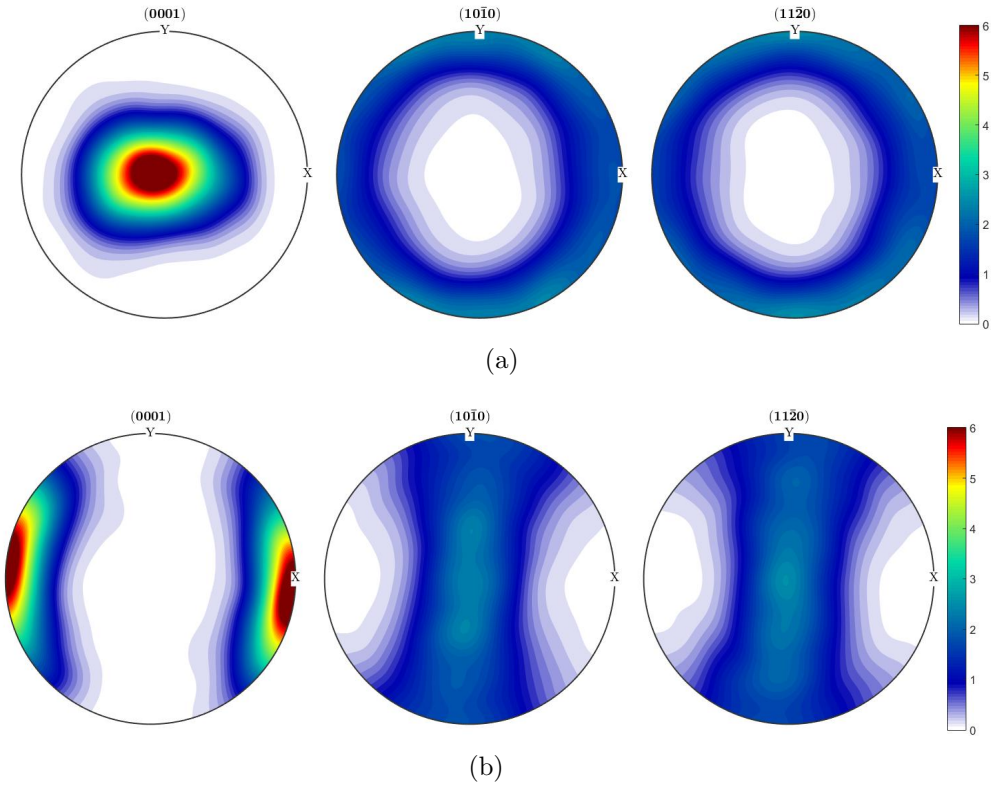

Fig. S1: (0001), (10$\bar{1}$0) *and* (11$\bar{2}$0) *pole figures pertaining to rolled AZ31 Mg alloy employed in experiments of Vaishakh et al. (2020) in (a) the TD-RD plane and (b) ND-TD plane.*

Fig. S1(a) and (b) display (0001), (10$\bar{1}$0) and (11$\bar{2}$0) pole figures of a rolled AZ31 Mg alloy in the TD-RD and ND-TD planes, respectively, constructed from about 5100 lattice

orientations, which are plotted using the MTEX software (Bachmann et al., 2010). From these figures, it is clear that most of the grains have their c-axis aligned close to ND, thereby resulting in a near-basal texture, which is expected for the rolled Mg alloy. By comparing Fig. S1(a) and (b) with Fig. 1(a) and (b) of the paper, which display the three pole figures in TD-RD and ND-TD planes, respectively pertaining to a statistically equivalent texture comprising of a reduced set of 100 orientations, it can be seen that they are quite similar.

S2. Determination of material constants for the polycrystal CPFE model

The material constants for various slip and twin systems are initially taken to be the same as those given by Selvarajou et al. (2017) for a polycrystalline Mg alloy. Then, the following sequence of steps is performed to tune the material parameters. First, the initial critical resolved shear stress (CRSS), τ_0, hardening modulus, h_0, and saturation shear stress, τ_s, corresponding to prismatic as well as basal slip are adjusted by matching the predicted and experimental stress-strain curves for RD and TD tension. Next, the parameters corresponding to TT, viz., h_{tt}, τ_{0-tt}, and τ_{s-tt}, are tuned based on the TD compression stress-strain curve, along with further alteration of parameters for basal slip. With the new material constants for TT and basal slip, the predicted TD tension stress-strain curve is again matched against the experimental variation by fine tuning τ_0, h_0 and τ_s of prismatic slip along with adjustment of twin-slip hardening moduli H_{c-s} and h_{t-s}. Finally, by comparing the simulated and experimental ND compression stress-strain curves, the parameters for pyramidal $\langle c+a \rangle$ slip as well as H_{ct} and b corresponding to CT are fixed. Since, the influence of pyramidal $\langle a \rangle$ slip on the stress-strain responses was marginal, the material parameters corresponding to this slip system are taken to be same as those given in Selvarajou et al. (2017).

S3. Estimation of material constants in the isotropic material model

For the SSY analysis using isotropic material model, the elastic constants are taken as the average of Young's modulus ($\bar{E}$) and Poisson's ratio ($\bar{\nu}$) from the elastic part of in-plane

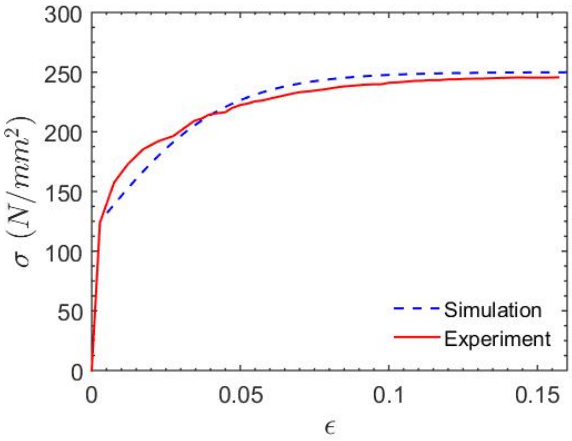

Fig. S2: *Comparison of stress-strain curve pertaining to RD tension obtained from FE simulation using isotropic von Mises material model along with saturation hardening law (Eq. (7) of the paper) and experimental data for the chosen Mg alloy.*

(TD-RD) tension and compression stress-strain curves obtained from CPFE analyses (refer Fig. 2). The values of $\bar{E}$ and $\bar{\nu}$, thus obtained, are 44500 N/mm^2 and 0.32, respectively. It is important to note that these values are quite close to the in-plane E and ν reported for a typical rolled polycrystalline Mg alloy. Also, as mentioned in Sec. 2.4 of the paper, the constants σ_i, σ_s and g_0 in the assumed hardening law (Eq. 7) are determined by matching the simulated uniaxial stress-strain curve with the experimental RD tension data. The comparison of the fitted curve with the experimental data for the above loading case is shown in Fig. S2 and can be seen to be quite good.

S4. Tensile twin volume fraction contours for mode I and II

The contours of net average tensile twin volume fraction (f_{tt}) at $|K|/(\sigma_0\sqrt{b_0}) = 14$ for $M_e = 1$ and 0, corresponding to TD-RD orientation, are displayed in normalized coordinates in Fig. S3(a), (b), respectively. Similar plots for the ND-TD orientation are presented in Fig. S3(c) and (d). It is important to note that the contour levels are higher and are also plotted over a substantially larger normalized distance in Fig. S3(c) and (d) (i.e., for the ND-TD orientation). From Fig. S3(a), (c), it can be noticed that the contours of f_{tt} for $M_e = 1$ bend backwards towards the notch flanks, and the peak values occur close to p and

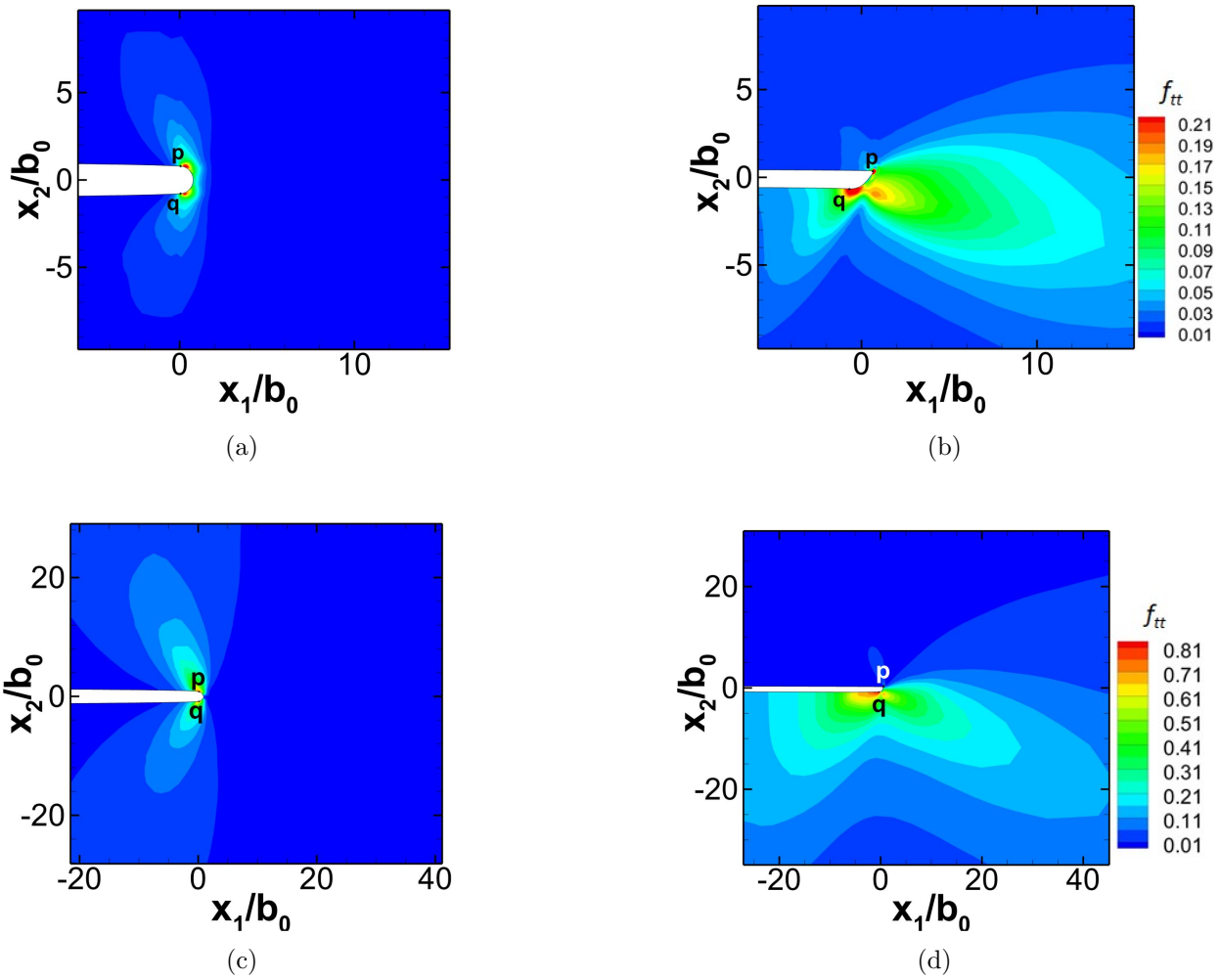

Fig. S3: *Contour plots of net average tensile twin volume fraction (f_{tt}) over a large region around the notch surface at $|K|/(\sigma_0\sqrt{b_0}) = 14$ obtained from CPFE simulations pertaining to TD-RD orientation for: (a) $M_e = 1$ and (b) $M_e = 0$. Similar plots for the ND-TD orientation are shown in (c) and (f).*

q. By contrast, f_{tt} contours spread out along the lower notch flank as well as ahead of the deformed notch surface for $M_e = 0$, similar to those for $M_e = 0.33$ presented in the paper. However, while the contours along the lower notch flank are more prominent for $M_e = 0.33$ (see Fig. 11 of the paper), those extending ahead of the notch tip are more noticeable for $M_e = 0$ (Fig. S3(b), (d)). Further, the f_{tt} contours for pure mode II loading bend towards the lower-half of the domain especially for the ND-TD orientation (Fig. S3(d)). Thus, for a given mode mixity, the overall spread of net average f_{tt} corroborates with the corresponding plastic zone shapes and sizes as can be perceived by comparing Fig. S3 with Fig. 5 of the paper.

S5. Tuning of fracture parameters

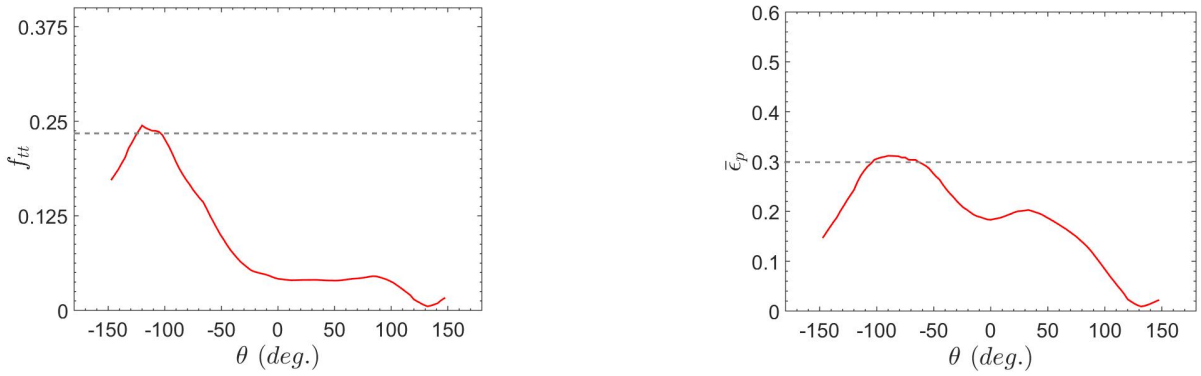

(a) (b)

Fig. S4: *Angular variation at a radial distance of $r_0 = 200$ μm from the notch tip (in undeformed configuration) corresponding to $M_e \sim 0.7$ and $J_c = 45$ N/mm of: (a) f_{tt} and (b) $\bar{\epsilon}_p$. The chosen critical levels of the above quantities (Table 2 of the paper) are indicated by dashed lines.*

The angular variations of f_{tt} and $\bar{\epsilon}_p$ at $r = r_{cv} = 0.2$ mm from the notch tip (in the undeformed configuration) are shown in Fig. S4(a) and (b), respectively, corresponding to $M_e \sim 0.7$ and $J = 45$ N/mm. Here, θ is measured counter-clockwise from the line directly ahead of the notch tip. From this figure, it can be seen that the peak values of $\bar{\epsilon}_p$ and f_{tt} are 0.3 and 0.24, respectively, and are attained in the lower portion of the specimen (i.e., $\theta < 0$) where pronounced stretching of the notch surface takes place. Therefore, these values are chosen as critical levels in Table 2 of the paper.

S6. Contour plots of $E_{r\theta}$ and $\sigma_{r\theta}$ for mixed-mode specimen

The contour plots of macroscopic Lagrangian shear strain, $E_{r\theta}$, and the macroscopic shear stress, $\sigma_{r\theta}$, obtained from the SSY simulation for TD-RD case, corresponding to $M_e = 0.67$, at $J = J_c = 45$ N/mm are displayed in normalized coordinates in Fig. S5(a) and (b), respectively. In these figures, the putative crack path originating from the notch surface, as observed in experiments, is indicated by a small black dashed line. It can be noticed from Fig. S5(a) and (b) that the crack path coincides with the macroscopic stress and strain state following $E_{r\theta} = 0$ and $\sigma_{r\theta} = 0$.

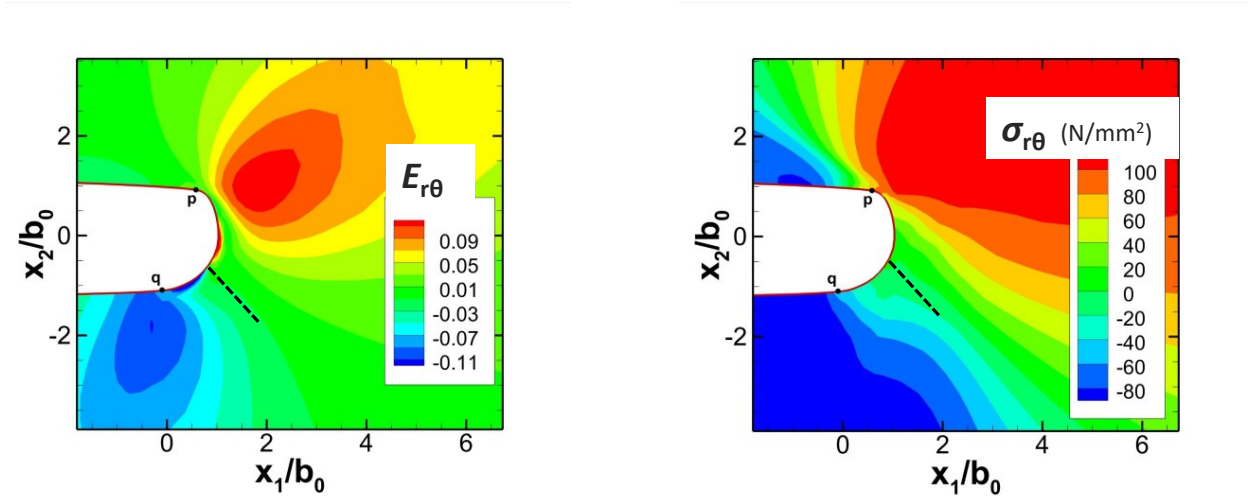

(a) (b)

Fig. S5: *Contour plots of (a) macroscopic Lagrangian shear strain component, $E_{r\theta}$ and (b) shear stress, $\sigma_{r\theta}$ at crack initiation stage ($J \sim 45$ N/mm) obtained from the SSY simulation corresponding to $M_e = 0.67$ for TD-RD orientation.*

References

Bachmann, F., Hielscher, R., Schaeben, H., 2010. Texture analysis with mtex – free and open source software toolbox, in: Texture and Anisotropy of Polycrystals III, Trans. Tech. Publ. Ltd. pp. 63–68.

Selvarajou, B., Joshi, S.P., Benzerga, A.A., 2017. Three dimensional simulations of texture and triaxiality effects on the plasticity of magnesium alloys. Acta Mater. 127, 54–72.

Vaishakh, K.V., Narasimhan, R., Yazar, K.U., Suwas, S., 2020. Mixed-mode (I and II) fracture behavior of a basal-textured magnesium alloy. Acta Mater. 193, 99–114.